Nanotubes

DOI: 10.1002/ange.200602636

Single-Crystal Nanotubes of II_3–V_2 Semiconductors**

Guozhen Shen, Yoshio Bando, Changhui Ye, Xiaoli Yuan, Takashi Sekiguchi, and Dmitri Golberg*

In recent years, considerable attention has been paid to 1D nanostructures, such as wires, rods, belts, ribbons, and tubes owing to their unique physical and chemical properties and potential applications in nanoscale devices with diverse functions.[1] In particular, since the first identification of carbon nanotubes in 1991,[2] much effort has been made to synthesize inorganic nanotubes controllably. A variety of nanotubes based on layered, or pseudolayered materials have been prepared, which include transition-metal chalcogenides (for example, MX_2,[3,4] where M is Mo or W, X is S or Se; and others[5,6]), $NiCl_2$,[7] BN,[8] vanadium oxide,[9] and Bi.[10] Synthesis of single-crystal nanotubes with nonlayered crystal structures was pioneered by Yang and co-workers, who prepared single-crystal GaN nanotubes by an "epitaxial casting" template process;[11] other nanotubes, such as Si and ZnS,[12] have since been obtained by using the same concept.

Semiconducting II_3–V_2 compounds are of scientific and technological importance because they have narrow band gaps. For example, the band gap of Cd_3P_2 is 0.55 eV and Zn_3P_2 has a band gap of 1.55 eV.[13] Owing to the large excitonic radii of these materials, they are expected to exhibit pronounced size quantization effects. The electrons in such a semiconductor will be confined in crystals that are much larger than if they were in analogous II–VI or III–V semiconductors. Bulk II_3–V_2 semiconductors have many potential applications in infrared detectors, lasers, solar-cell technology, ultrasonic multipliers, and Hall generators.[14] However, compared with the significant progress in 1D nanoscale II–VI and III–V semiconductors, research on nanoscale II_3–V_2 semiconductors has been lagging far behind because of the lack of general synthetic methods. To date, there are only a few reports on the synthesis of 0D II_3–V_2 nanoparticles by using metal–organic processes,[15] and no reports on 1D II_3–V_2 nanostructures. Very recently, we synthesized 1D trumpetlike Zn_3P_2 nanostructures by using a thermochemical process.[16] This success inspired us to attempt further efforts in synthesizing hollow nanotubes of II_3–V_2 semiconductors because nanotubes have certain properties that are superior to their nanowire counterparts. For example, hollow nanotubes can serve as nanoscale containers or pipes to deliver fluids and molecular species. They are excellent building blocks for the construction of large-scale nanofluidic systems.[17]

Herein, we report the first synthesis of single-crystal II_3–V_2 nanotubes. Nanotubes of Cd_3P_2 and Zn_3P_2 semiconductors are synthesized by a template process, in which the in situ formed Cd or Zn nanorods act as the self-sacrificing templates for the growing nanotubes. By carefully controlling the experimental parameters, II_3–V_2 nanotube-based 1D heterostructures are also fabricated by using this simple method.

Single-crystal Cd_3P_2 and Zn_3P_2 nanotubes were synthesized at 1350 °C under ambient pressure in a vertical induction furnace from a mixture of CdS (or ZnS), P, and Mn_3P_2 powders. After the reaction had finished, woollike material was collected from the inner wall of the graphite cylinder of the apparatus. The phase composition and structure of the product were examined by powder X-ray diffraction (XRD; Figure 1). As shown in Figure 1a, all the reflection peaks in

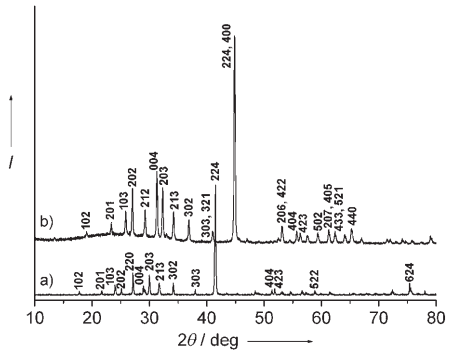

Figure 1. XRD patterns of a) Cd_3P_2 nanotubes and b) Zn_3P_2 nanotubes.

this pattern can be readily indexed to tetragonal phase (space group $P4_2/nmc$) of Cd_3P_2 phase (JCPDS Card No. 65-2856). The pattern in Figure 1b can be indexed to tetragonal (space group $P4_2/nmc$) Zn_3P_2 (JCPDS Card no. 65-2854). During XRD, no characteristic peaks from other crystalline impurities, such as Mn_3P_2, MnP, Zn, ZnS, (or Cd, CdS), were detected, thus indicating the formation of pure products.

Field-emission scanning electron microscopy (FESEM) was used to examine the morphology of the products. Figure 2a shows a low-magnification SEM image of as-synthesized Cd_3P_2 product. The product consists exclusively of 1D wirelike nanostructures with lengths ranging from several tens to hundreds of micrometers. A high-magnification SEM image (Figure 2b) reveals hollow 1D nanostructures. Typically, these Cd_3P_2 nanotubes have outer diameters of 80–250 nm and very thin walls. All the obtained nanotubes had open ends without any attached particles (inset of

[*] Dr. G. Shen, Prof. Y. Bando, Dr. C. Ye, Prof. D. Golberg
Nanoscale Materials Center
National Institute for Materials Science (NIMS)
Namiki 1-1, Tsukuba, Ibaraki 305-0044 (Japan)
Fax: (+81) 298-513-354
E-mail: shen.guozhen@nims.go.jp
Dr. X. Yuan, Prof. T. Sekiguchi
Advanced Electronic Materials Center
National Institute for Materials Science (NIMS)
Namiki 1-1, Tsukuba, Ibaraki 305-0044 (Japan)

[**] We thank Y. Uemura and K. Kurashima for their help in the setup of experiments and TEM work, and Dr. C. Y. Zhi for helpful discussions. II and V indicate elements of Group II and Group V, respectively, of the periodic table.

Supporting information for this article is available on the WWW under http://www.angewandte.org or from the author.

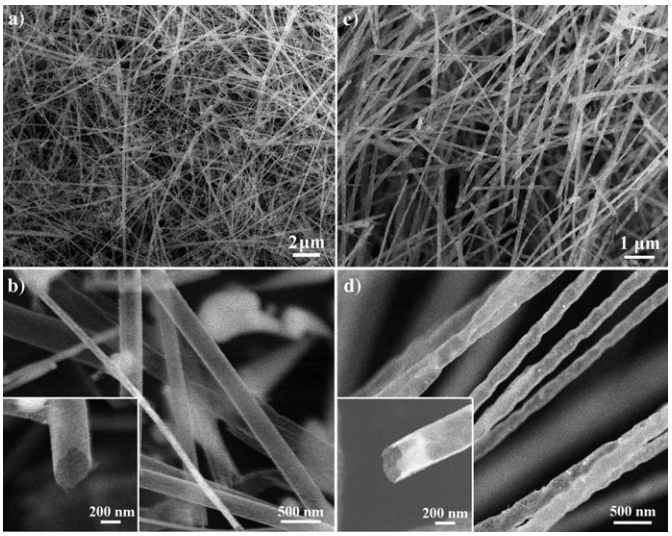

Figure 2. SEM images of a,b) Cd_3P_2 nanotubes and c,d) Zn_3P_2 nanotubes at different magnifications, see text for details.

Figure 2b). An SEM image of the Zn_3P_2 product is shown in Figure 2c, which also documents the formation of 1D wirelike nanostructures with lengths of tens of micrometers. High-magnification SEM images give clear evidence of Zn_3P_2 nanotube formation (Figure 2d and inset). The nanotube outer diameters are in the range of 100–200 nm. As with the Cd_3P_2 nanotubes, all the Zn_3P_2 nanotubes had open tips without any attached particles.

The morphology and composition of the products were further investigated by using transmission electron microscopy (TEM) and energy-dispersive X-ray spectrometry (EDS). Figure 3a shows the low-magnification TEM image of the Cd_3P_2 product and the formation of smooth nanotubes with outer diameters of 80–250 nm, which is in accordance with the SEM results. Figures 3b and c depict the tip ends of the Cd_3P_2 nanotubes: the nanotubes have circular cross sections, open ends without any attached particles, uniform diameters along their entire lengths, and very thin walls. Some partially filled nanotubes were also found (TEM images in Figures 3d and e). EDS spectra of the nanotube walls and the inner filler material were analyzed to check their compositions. The EDS spectrum of a nanotube in Figure 3f shows that the nanotube is composed of Cd and P atoms with an approximate atomic ratio of 1.62:1, which is close to the stoichiometry of Cd_3P_2. In this spectrum, the signals corresponding to Cu arise from the TEM grid. No other impurity was detected. Figure 3g shows the main signal of elemental Cd as well as a weak signal of P, which indicates that the filler material is Cd. Thus, the partially filled structures are Cd-filled Cd_3P_2 nanotubes.

Further detailed structural analysis of the products was carried out by using high-resolution TEM (HRTEM) and selected-area electron diffraction (SAED). Figures 4a and b are the low-magnification TEM images of two typical Cd_3P_2 nanotubes without any filling material. The corresponding SAED pattern in the inset of Figure 4b indicates their single-crystal nature. TEM confirmed that all the Cd_3P_2 nanotubes have very thin walls with respect to their diameters. Figure 4c

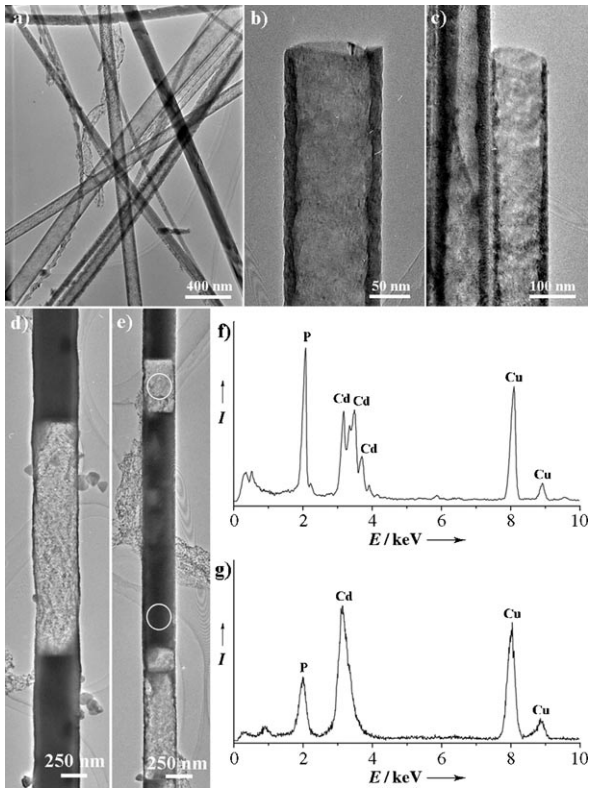

Figure 3. a) TEM image of Cd_3P_2 nanotubes. b,c) TEM images showing the tips of the Cd_3P_2 nanotubes. d,e) TEM images of Cd-filled Cd_3P_2 nanotubes. f,g) EDS spectra of the parts circled in (e), see text for details.

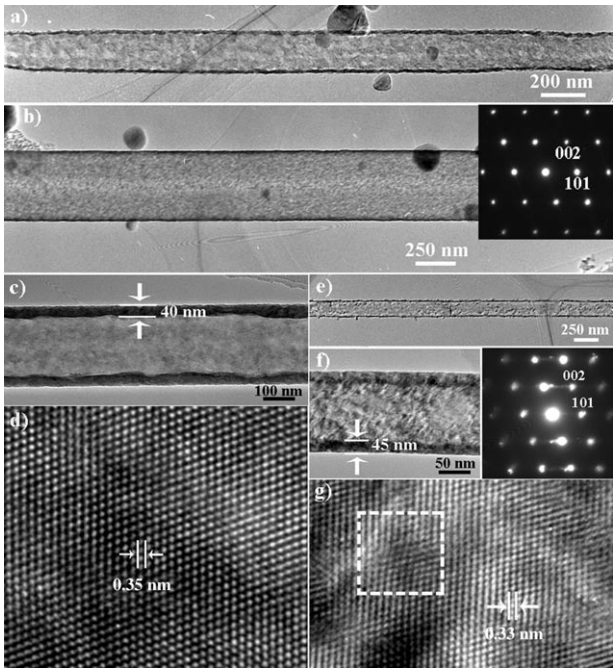

Figure 4. a,b) TEM image of Cd_3P_2 nanotubes and corresponding SAED pattern (inset). c) HRTEM image showing the wall thickness of a Cd_3P_2 nanotube. d) Lattice-resolved HRTEM image of a Cd_3P_2 nanotube. e) Low-magnification TEM image of a Zn_3P_2 nanotube. f) HRTEM image showing the wall thickness of a Zn_3P_2 nanotube and its SAED pattern. g) Lattice-resolved HRTEM image of a Zn_3P_2 nanotube, marked area shows evidence of defects.

shows a high-magnification (HR) TEM image of a single Cd_3P_2 nanotube with a diameter around 250 nm and wall thickness around 40 nm. A lattice-resolved HRTEM image of the Cd_3P_2 nanotube is given in Figure 4d; the clearly marked interplanar *d* spacing is 0.35 nm, which corresponds to that of the {202} lattice planes of tetragonal Cd_3P_2. In light of the SAED pattern in Figure 4b, the HRTEM result indicates that each Cd_3P_2 nanotube is a single crystal with the preferred growth direction perpendicular to the (101) planes.

Structural information on the Zn_3P_2 nanotubes was obtained by HRTEM analysis. Figure 4e is the TEM image of a single Zn_3P_2 nanotube with an outer diameter of approximately 150 nm; the hollow cavity can be clearly seen. All of the nanotubes are thin, with wall thickness of 5–50 nm. An HRTEM image (Figure 4f) shows a nanotube with a wall thickness of approximately 45 nm. An SAED pattern of the Zn_3P_2 (inset of Figure 4f) confirms that the nanotubes are single-crystalline. Streaks parallel to the growth direction of the Zn_3P_2 nanotube are visible, which indicates the presence of defects within the nanotube. Figure 4g is a lattice-resolved HRTEM image taken of the Zn_3P_2 nanotubes. The lattice spacing of 0.33 nm perfectly matches the {202} lattice planes of tetragonal Zn_3P_2. These fringes are perpendicular to the nanotube axis. The results indicate that the Zn_3P_2 nanotube also has a preferred growth direction perpendicular to the (101) planes, which is similar to that of the Cd_3P_2 nanotubes. Defects, such as dislocations were observed in the nanotube as see in the marked area of the image.

To gain insight into the growth process of II_3–V_2 nanotubes, we performed a series of experiments in which the quantity of reagents, reaction temperature, and time were varied. Figure 5a shows an SEM image of a product when a mixture of ZnS, P, and Mn_3P_2 with a molar ratio of 5:1:1 was used. 1D nanostructures were still formed under these conditions. However, a high-magnification SEM image (Figure 5b) shows that they are of hierarchical branch–stem morphology. TEM and EDS analyses demonstrate interesting hierarchical ZnS nanowire (branches) and Zn_3P_2 nanotube (stems) heterostructures (see Supporting Information). When the amount of ZnS in the mixture was further increased, Zn_3P_2 nanotubes coated with ZnS nanoparticles were obtained instead of pure Zn_3P_2 nanotubes (Figures 5c and d). The reaction temperature is another key factor that influences product morphology. Figures 5e and 5f depict the SEM images of a product synthesized at about 1500 °C. Clearly, the products comprise Zn_3P_2 microtubes with open tips and diameters around 1 μm.

During the formation of Zn_3P_2 nanotubes, most of the nanotubes obtained 20 min after the start of the reaction were filled with Zn metal (Figures 5g and h). With a prolongation of the reaction time, the Zn inside the nanotubes was consumed through evaporation to leave hollow nanotubes. Similar processes were also observed for the formation of Cd_3P_2 nanotubes. Based on these findings, we propose a self-sacrificing template mechanism to explain the formation of the nanotubes. At a high temperature, M′S (M′ = Zn, Cd) reacts with C (from the graphite crucible) by the reaction $2M'S + C \rightarrow 2M' + CS_2$ to produce gaseous M′. Gaseous M′ is transferred by the carrier gas (N_2) to the low-temperature region, where it is deposited on the graphite crucible (Figure 6a). Owing to the anisotropic nature of wurtzite M′ phases, 1D M′ nanorods are rapidly formed (Figure 6b). At the same time, Mn_3P_2 also decomposes to generate gaseous P, which is also transferred to the low-temperature region, where it reacts with the M′ nanorods by $3M' + 2P \rightarrow M'_3P_2$, and thus coaxial M′/$M'_3P_2$ nanocables are produced (Figure 6c). During this process, the dislocations formed in the M'_3P_2 relax the built-in strain, which is confirmed by the presence of dislocations in the synthesized

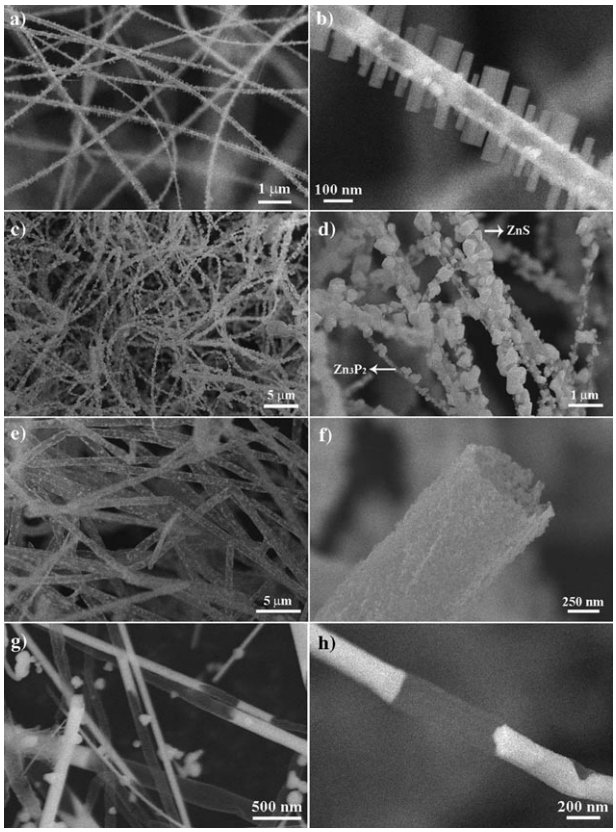

Figure 5. FESEM images of Zn_3P_2 products prepared under different conditions (see text for details): a,b) hierarchical structures of Zn_3P_2 nanotubes with ZnS nanowire branches; c,d) Zn_3P_2 nanotubes coated with ZnS nanoparticles; e,f) Zn_3P_2 microtubes. g,h) SEM images of the partially filled Zn_3P_2 nanotubes.

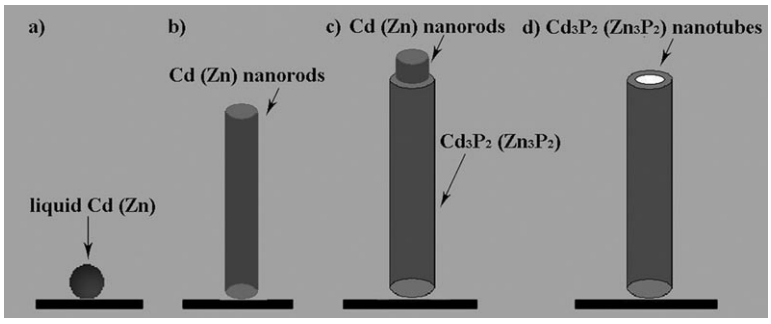

Figure 6. Proposed growth mechanism of the II_3–V_2 nanotubes, see text for details.

products (Figure 4g). After a reaction time, the M′ species is partially consumed through evaporation out of the coaxial nanocables, whereas the M'_3P_2 shell remains intact, and single-crystalline M'_3P_2 nanotubes with circular cross sections are formed (Figure 6d).

The cathodoluminescence (CL) properties of II_3–V_2 nanotubes have been studied at 16 K. The samples were first deposited on a standard copper TEM grid and thoroughly characterized by TEM before they were set into the CL system. CL spectra from individual nanotubes were obtained with a high-resolution CL system that operates at an accelerating voltage of 5 kV and a current of 1.2 nA in a low-energy CL system inside a thermal field-emission scanning electron microscope (TFESEM, Hitachi S4200). Figure 7

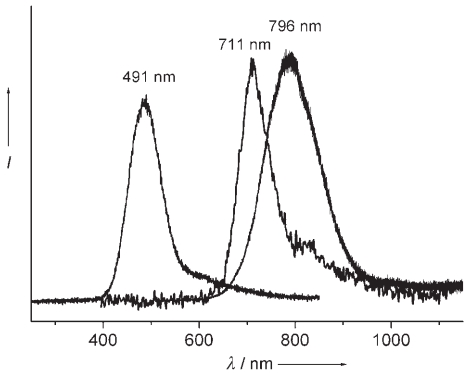

Figure 7. CL spectra of II_3–V_2 nanotubes with wall thicknesses of about 10, 20, and 45 nm, with emissions at 491, 711, and 796 nm, respectively.

shows the CL spectra taken from Zn_3P_2 nanotubes with different wall thickness of about 10, 20, and 45 nm; emissions centered at about 491, 711, and 796 nm were observed, respectively. Emissions from nanotubes with wall thickness of 10 and 20 nm were blue-shifted with respect to the emission of bulk Zn_3P_2 (1.55 eV, 802 nm). It has been reported that the emission values increase from nanoparticles with respect to those from the bulk crystal because of quantum confinement in the nanoparticles.[15c] For example, photoluminescence (PL) studies indicate that Zn_3P_2 quantum dots with different diameters show emissions ranging from 2.74 eV (450 nm) to 3.55 eV (349 nm), which are greatly blue-shifted compared to the standard emission values from bulk crystals.[15c] For synthesized Zn_3P_2 nanotubes, we think that the blue-shift of emissions observed for nanotubes with thin walls is caused by quantum confinement.[15] For the nanotubes with thicker walls (45 nm), no appreciable shift is observed as the walls are larger than the excitonic radii. CL properties of the Cd_3P_2 nanotubes were also checked, but no obvious CL emission was observed.

In conclusion, we have synthesized single-crystal II_3–V_2 nanotubes (Cd_3P_2 and Zn_3P_2) through a thermochemical process and characterized them by XRD, SEM, TEM, and EDS studies. A self-sacrificing template mechanism is proposed to explain nanotube formation, which involves the in situ step-by-step formation of Group IIB metal nanorods, Group IIB metal cores, II_3–V_2 semiconductor shells, and finally II_3–V_2 nanotubes. By carefully controlling the experimental parameters, this simple method can be used to prepare diverse II_3–V_2 nanotube-based 1D heterostructures. Furthermore, with judicious choice of source materials, II_3–V_2 nanotubes with compositions other than Cd_3P_2 and Zn_3P_2, such as Cd_3As_2 and Zn_3As_2, may be fabricated.

Experimental Section

Single-crystal nanotubes of Zn_3P_2 and Cd_3P_2 semiconductors were synthesized in a vertical induction furnace, which consists of a fused-quartz tube and an induction-heated cylinder made of high-purity graphite coated with a carbon-fiber thermo-insulating layer. The furnace has one inlet C pipe and one outlet C pipe on its base. In a typical process, a graphite crucible that contains a mixture of ZnS (or CdS), P, and Mn_3P_2 powders with a molar ratio of 3:1:1 was placed in the center cylinder. After evacuation of the quartz tube to approximately 20 Pa, a flow of pure N_2 was introduced and maintained through the inlet at a flow rate of 50 standard cubic centimeters per minute (sccm) at ambient pressure in the furnace, and the crucible was rapidly heated and kept around 1350 °C for 1 h. After the reaction was terminated and the furnace cooled to room temperature, woollike products had deposited on the inner wall of the graphite cylinder. The collected products were characterized by X-ray diffraction (XRD, RINT 2200HF), SEM (JSM-6700F), and HRTEM (JEM-3000F) equipped with an energy-dispersive X-ray spectrometer (EDS).

Received: July 3, 2006
Revised: August 23, 2006
Published online: October 18, 2006

Keywords: chemical vapor deposition · nanotechnology · nanotubes · scanning probe microscopy · template synthesis

[1] a) J. T. Hu, T. W. Odom, C. M. Lieber, *Acc. Chem. Res.* **1999**, *32*, 435–445; b) Y. N. Xia, P. D. Yang, Y. Sun, Y. Wu, B. Mayers, B. Gates, Y. Yin, F. Kim, H. Yan, *Adv. Mater.* **2003**, *15*, 353–389.
[2] S. Iijima, *Nature* **1991**, *354*, 56–58.
[3] a) R. Tenne, L. Margulis, M. Genut, G. Hodes, *Nature* **1992**, *360*, 444–446; b) Y. Feldman, E. Wasserman, D. J. Srolovitz, R. Tenne, *Science* **1995**, *267*, 222–225.
[4] a) R. Tenne, *Prog. Inorg. Chem.* **2001**, *50*, 269–315; b) R. Tenne, A. Zettl, *Top. Appl. Phys.* **2001**, *80*, 81–112; c) R. Tenne, *Chem. Eur. J.* **2002**, *8*, 5297–5304.
[5] a) M. Nath, C. N. R. Rao, *J. Am. Chem. Soc.* **2001**, *123*, 4841–4842; b) M. Nath, C. N. R. Rao, Angew. Chem. **2002**, *114*, 3601–3604; *Angew. Chem. Int. Ed.* **2002**, *41*, 3451–3454; c) U. K. Gautam, S. R. C. Vivekchand, A. Govindaraj, G. U. Kulkarni, N. R. Selvi, C. N. R. Rao, *J. Am. Chem. Soc.* **2005**, *127*, 3658–3659.
[6] a) C. H. Ye, G. W. Meng, Z. Jiang, Y. H. Wang, G. Wang, L. D. Zhang, *J. Am. Chem. Soc.* **2002**, *124*, 15180–15181; b) J. Yang, Y. C. Liu, H. M. Lin, C. C. Chen, *Adv. Mater.* **2004**, *16*, 713–716.
[7] Y. R. Hacohen, E. Grunbaum, R. Tenne, J. Sloan, J. L. Hutchison, *Nature* **1998**, *395*, 336–337.
[8] N. G. Chopra, R. J. Luyken, K. Cherrey, V. H. Crespi, M. L. Cohen, S. G. Louie, A. Zettl, *Science* **1995**, *269*, 966–967.
[9] a) M. E. Spahr, P. Bitterli, R. Nesper, M. Müller, F. Krumeich, H.-U. Nissen, *Angew. Chem.* **1998**, *110*, 1339–1342; *Angew. Chem. Int. Ed.* **1998**, *37*, 1263–1266; b) G. R. Patzke, F. Krumeich, R. Nesper, *Angew. Chem.* **2002**, *114*, 2554–2571; *Angew. Chem. Int. Ed.* **2002**, *41*, 2446–2453.
[10] Y. D. Li, J. W. Wang, Z. X. Deng, Y. Y. Wu, X. M. Sun, D. P. Yu, P. D. Yang, *J. Am. Chem. Soc.* **2001**, *123*, 9904–9905.

[11] J. Goldberger, R. He, Y. Zhang, S. Lee, H. Q. Yan, H. J. Choi, P. D. Yang, *Nature* **2003**, *422*, 599 – 602.
[12] a) Z. Q. Liu, D. H. Zhang, S. Han, C. Li, B. Lei, W. G. Lu, J. Y. Fang, C. W. Zhou, *J. Am. Chem. Soc.* **2005**, *127*, 6 – 7; b) J. Q. Hu, Y. Bando, Z. W. Liu, J. H. Zhan, D. Golberg, T. Sekiguchi, *Angew. Chem.* **2004**, *116*, 65 – 68; *Angew. Chem. Int. Ed.* **2004**, *43*, 63 – 66; c) J. Q. Hu, Y. Bando, J. H. Zhan, D. Golberg, *Angew. Chem.* **2004**, *116*, 4706 – 4709; *Angew. Chem. Int. Ed.* **2004**, *43*, 4606 – 4609.
[13] O. Madelung, *Data in Science and Technology: Semiconductors other Than Group IV Elements and III–V Compounds*, Springer, Berlin.
[14] a) W. Zdanowicz, L. Zdanowicz, *Annu. Rev. Mater. Sci.* **1975**, *5*, 301 – 328; b) E. K. Arushanov, *Prog. Cryst. Growth Charact.* **1980**, *3*, 211 – 255; c) V. B. Larzarev, V. Y. Schevchenka, Y. H. Greenberg, V. V. Sobolein, *II–V Semiconducting Compounds*, Nauska, Moscow, **1978**; d) M. Bushan, A. Catalano, *Appl. Phys. Lett.* **1981**, *38*, 39 – 41.
[15] a) M. Green, P. O'Brien, *Adv. Mater.* **1998**, *10*, 527 – 528; b) M. Green, P. O'Brien, *J. Mater. Chem.* **1999**, *9*, 243 – 247; c) M. Green, P. O'Brien, *Chem. Mater.* **2001**, *13*, 4500 – 4505; d) H. Weller, A. Fojtik, A. Henglein, *Chem. Phys. Lett.* **1985**, *117*, 485 – 487; e) S. C. Goel, M. Y. Chang, W. E. Buhro, *J. Am. Chem. Soc.* **1990**, *112*, 5636 – 5637.
[16] G. Z. Shen, Y. Bando, J. Q. Hu, D. Golberg, *Appl. Phys. Lett.* **2006**, *88*, 143105.
[17] a) R. Fan, R. Karnik, M. Yue, D. Y. Li, A. Majumdar, P. D. Yang, *Nano Lett.* **2005**, *5*, 1633 – 1637; b) J. Goldberger, R. Fan, P. D. Yang, *Acc. Chem. Res.* **2006**, *39*, 239 – 248; c) R. Fan, M. Yue, R. Karnik, A. Majumdar, P. D. Yang, *Phys. Rev. Lett.* **2005**, *95*, 086607.

